Bulky anion effect on the architecture of chiral dysprosium single-molecule magnets

Haiet Douib, Kais Dhbaibi, Bertrand Lefeuvre, Vincent Dorcet, Thierry Guizouarn, Fabrice Pointillart

Bulky Anion Effect on the Architecture of Chiral Dysprosium Single-Molecule Magnets

Haiet Douib,[1,2] Kais Dhbaibi,[1] Bertrand Lefeuvre,[1] Vincent Dorcet,[1] Thierry Guizouarn,[1] Fabrice Pointillart*[1]

[1] *Univ Rennes, CNRS, ISCR (Institut des Sciences Chimiques de Rennes) – UMR 6226, 35000 Rennes (France)*

E-mail: fabrice.pointillart@univ-rennes1.fr

[2] *Laboratoire des Matériaux Organiques et Hétérochimie (LMOH), Département des sciences de la matière, Université Larbi Tébessi de Tébessa, Route de Constantine 12002, Tébessa, Algérie.*

Abstract

The interest for chiral tris(β-diketonato)lanthanide complexes in coordination chemistry is huge due to its Lewis acid character, optical activity and the control of the final compound architecture. However, it could limit the possibilities of molecular architectures which could be obtained. A pair of enantiomers for dinuclear complexes $[Dy((-)/(+)hfc)_3(\mathbf{L})]_2{\cdot}C_7H_{16}$ **([(-)/(+)1]**$\cdot C_7H_{16}$) (**L** = 4′-(4′′′-pyridyl-*N*-oxide)-1,2′:6′1′′-bis-(pyrazolyl)pyridine]) was obtained while the presence of bulky BArF anions led to a partial dissociation of the chiral $[Dy((-)/(+)hfc)_3(H_2O)]$ (hfc^- = 3-(heptafluoropropylhydroxymethylene)-(+/-)-camphorate) and the formation of mono-dimensional cationic chiral polymer $\{[Dy((-)/(+)hfc)_2(\mathbf{L})][BarF]\}_n{\cdot}nCH_3NO_2$ **[(-)/(+)2]$_n$**$\cdot nCH_3NO_2$). Natural circular dichroism (NCD) highlighted an exciton CD couplet for **[(-)/(+)2]$_n$** but not for **(-)/(+)1**. The latter behaves as a Single-Molecule Magnet (SMM) with a blocking temperature up to 4 K while **[(-)/(+)2]$_n$** is a 1D assembly of field-induced SMMs with a magnetic relaxation occurring through a Raman process only.

Keywords: β-diketonate, dipyrazolylpyridine, Dysprosium, Chirality, Circular Dichroism, Single-Molecule Magnet

1. INTRODUCTION

One of the most convenient synthetic way to observe Single-Molecule Magnet (SMM) behavior and luminescence is the combination of organic chromophores and lanthanide ions using coordination chemistry approach.[1,2] Indeed, lanthanide ions possess intrinsic high magnetic moment and strong magnetic anisotropy and specific optical characteristics such as narrow emission bands and long lifetime making them ideal candidates for such purposes. The Ising-type magnetic anisotropy could be optimized by controlling the crystal field and the electronic distribution of the coordination sphere to give few year ago the first SMM displaying a blocking temperature at liquid nitrogen temperature.[3] Such magnetic bistability at the molecular scale opens the door to potential applications in high density data storage.[4] A great challenge for both chemist and physicist communities is the combination of two or more physical properties in an unique molecular systems which could allow the observation of new physical properties. In particular, the addition of the chirality to magnetism leads to appearance of ferroelectricity[5] and Magneto-Chiral Dichroism (MChD)[6] as recently observed by some of us in lanthanide coordination complexes[7]. The chirality can come from the organic ligands,[8-11] from their arrangement around the lanthanide center[12] or from both[13]. In order to better control the molecular architecture of the final compound, a well-known strategy is to use metallic precursors involving blocking ligands such as the neutral Ln(β-diketonate)$_3$ where the β-diketonate could be the chiral 3-trifluoro-acetyl-(+/-)-camphorato (facam$^-$) or 3-(heptafluoropropylhydroxymethylene)-(+/-)-camphorate (hfc$^-$) anions. In these complexes, the β-diketonate is sufficiently labile to permit the modulation of the number of β-diketonate in function of the presence of cations[14-16] or anions[17,18] in order to guaranty the neutrality of the final compounds. In other words, complexes of formula (C)(Ln(β-diketonate)$_4$) and (Ln(β-diketonate)$_2$(A)$_n$) are formed in presence of cation (C+) or anion (A-).

In the present article, the ligand [4′-(4′′′-pyridyl-*N*-oxide)-1,2′:6′1′′-bis-(pyrazolyl)pyridine] (**L**) was synthetized. **L** is a multi-coordination sites ligand with a mono- and tris-chelating moieties suitable to coordinate both lanthanide and transition metal. Indeed, the tris-chelating dipyrazolylpyridine (dpp) is well-known to coordinate lanthanide ions for slow magnetic relaxation[19] as well as transition metal, especially Fe(II), for spin-crossover behavior[20,21]. The mono-chelating pyridine-*N*-oxide group (NO) is mainly use to connect lanthanide ions.[17,18,22-24] The Dy(hfc)$_3$(H$_2$O) precursor was associated with an equimolar quantity of ligand (**L**) (Scheme 1) leading to the formation of a dinuclear complex of formula [Dy((-)/(+)hfc)$_3$(**L**)]$_2$·C$_7$H$_{16}$ (**[(-)/(+)1**]·C$_7$H$_{16}$) while in presence of the bulky tetrakis[3,5-

bis(trifluoromethyl)phenyl]borate (BArF) anion, a cationic coordination polymer of formula $\{[Dy((-)/(+)hfc)_2(\mathbf{L})][BarF]\}_n \cdot nCH_3NO_2$ **$([(-)/(+)2]_n \cdot nCH_3NO_2)$** is isolated. The single crystal molecular structures, electronic circular dichroism and magnetic behavior were investigated for both **(+)1** and **$[(+)2]_n$**.

2. MATERIALS AND METHODS

The precursors $Dy((-)/(+)hfc)_3(H_2O)$ (hfc^- = 3-(heptafluoropropylhydroxymethylene)-(+/-)-camphorate anion) were synthesized following previously reported methods.[25] All other reagents were purchased from Merck Co., Inc. and used without further purification. All solid-state characterization studies (elementary analysis, IR, PXRD and magnetic susceptibility measurements) were performed on dried samples and are considered without solvent of crystallization. The elemental analyses of the compounds were performed at the Centre Régional de Mesures Physiques de l'Ouest, Rennes.

2.1 Preparation of the ligand 4′-(4‴-pyridyl-*N*-oxide)-1,2′:6′1″-bis-(pyrazolyl)pyridine] (L)

To a cold $CHCl_3$ solution (60 mL, 0°C) containing 500 mg of 4′-(4‴-pyridyl)-1,2′:6′1″-bis-(pyrazolyl)pyridine][26] (1.73 mmol) was added drop by drop 15 mL of $CHCl_3$ of *m*CPBA (1.79g, 70%). After the addition, the resulting solution was stirred overnight at room temperature and then concentrated to about 15 mL. The crude ligand was purified by chromatography on neutral alumina with $CHCl_3$ as eluent to give white off microcrystalline powder of pure **L**. Yield 358 mg (68%). Anal. Calcd (%) for $C_{16}H_{12}N_6O$ (**L**): C 63.09, H 3.94, N 27.60; found: C 62.89, H 3.99, N 27.55. ^{1}H NMR ($CDCl_3$): δ=8.62 (dd, 2H), 8.34 (d, 2H), 8.11 (s, 2H), 7.82 (d, 2H), 7.77 (dd, 2H), 6.56 (dd, 2H) ppm. Slow evaporation of a saturated solution of $CHCl_3$ gave colourless single crystals of **L** suitable for single-crystal X-ray diffraction study.

2.2 Preparation of the complexes $[Dy((-)/(+)hfc)_3(L)]_2 \cdot C_7H_{16}$ $[(-)/(+)1] \cdot C_7H_{16}$ and $\{[Dy((-)/(+)hfc)_2(L)][BArF]\}_n \cdot nCH_3NO_2$ $[(-)/(+)2]_n \cdot nCH_3NO_2$

$[Dy((-)/(+)hfc)_3(L)]_2 \cdot C_7H_{16}$ $[(-)/(+)1] \cdot C_7H_{16}$. 48.9 mg (0.04 mmol) of $[Dy((-/+)hfc)_3(H_2O)]$ were dissolved in 10 mL of CH_2Cl_2 and added to a solution containing 12.6 mg (0.04 mmol)

of **L** in 10 mL of CH_2Cl_2. After 30 minutes of stirring, 30 mL of *n*-heptane were layered. After several days, the solution was slowly evaporated leading to colorless single crystals of [**(-)/(+)1**]·C_7H_{16} suitable for X-ray diffraction studies. 51.1 mg, 82 % yield for [**(-)1**]·C_7H_{16} and 52.4 mg, 84 % yield for [**(+)1**]·C_7H_{16}. Anal. Calcd (%) for $C_{116}H_{108}Dy_2F_{42}N_{12}O_{14}$ ([**(-)1**]): C 46.13, H 3.60, N 5.57; found: C 46.27, H 3.64, N 5.49. Anal. Calcd (%) for $C_{116}H_{108}Dy_2F_{42}N_{12}O_{14}$ ([**(+)1**]): C 46.13, H 3.60, N 5.57; found: C 46.22, H 3.69, N 5.44. Representative I.R. (KBr; range 4000–400 cm^{-1}): 2968 (m), 2932 (w), 2879 (w), 1657 (s), 1550 (m), 1524 (m), 1346 (m), 1260 (s), 1230 (s), 1176 (s), 1115 (m), 1078 (w), 1041 (w), 952 (w), 897 (w), 781 (w), 749 (w) and 539 (w) cm^{-1}.

{[Dy((-)/(+)hfc)$_2$(L)][BarF]}$_n$·nCH$_3$NO$_2$ [(-)/(+)2]$_n$·nCH$_3$NO$_2$. A 10 mL CH_2Cl_2 solution of 12.6 mg (0.04 mmol) of **L** was added to 10 mL of CH_3NO_2 containing 70.9 mg of sodium tetrakis[3,5-bis(trifluoromethyl)phenyl]borate (NaBArF) (0.08 mg). After 2h of stirring at room temperature, 48.9 mg of [Dy(hfc)$_3$(H_2O)] (0.04 mmol) in 5 mL of CH_2Cl_2 was added to the previous solution and then added 30 minutes more. Slow evaporation of the mother solution led to light yellow single crystals which were suitable for X-ray studies. 65.0 mg, 78 % yield in crystals for **[(-)2]$_n$**·nCH_3NO_2 and 67.5 mg, 81 % yield in crystals for **[(+)2]$_n$**·nCH_3NO_2. Anal. calcd (%) for $C_{76}H_{50}BDyF_{38}N_6O_5$ **[(-)2]$_n$**: C 44.50, H 2.47, N 4.15; found: C 44.34, H 2.44, N 4.11. Anal. calcd (%) for $C_{76}H_{50}BDyF_{38}N_6O_5$ **[(+)2]$_n$**: C 44.50, H 2.47, N 4.15; found: C 44.31, H 2.41, N 4.17 Representative I.R (KBr, range 4000–400 cm^{-1}): 3139 (w), 2967 (m), 2878 (w), 1649 (s), 1532 (s), 1463 (w), 1415 (m), 1356 (s), 1280 (s), 1228 (s), 1176 (s), 1127 (s), 974 (m), 892 (m), 839 (m), 752 (m), 713 (m), 674 (m), 598 (m), 537 (w) and 488 (w) cm^{-1}.

2.3 X-ray Structure Analysis

Single crystal were mounted on a D8 VENTURE Bruker-AXS diffractometer for data collection for **L** (Table S1) and the two pairs of enantiomers [**(-)1**]·C_7H_{16} /[**(+)1**]·C_7H_{16} and **[(-)2]$_n$**·nCH_3NO_2/**[(+)2]$_n$**·nCH_3NO_2 (MoKα radiation source, λ = 0.71073 Å) from the Centre de Diffractométrie X (CDIFX), Université de Rennes 1, France. Structures were solved with direct methods using the SHELXT Program[27] and refined with a full matrix least-squares method on F2 using the SHELXL-14/7 program.[28] SQUEEZE procedure of PLATON[29] was performed for structures containing large solvent accessible voids in which residual peak of diffraction were observed. Crystallographic data are summarized in Tables S1 and S2.

Crystallographic data for the structure reported in this paper have been deposited with the Cambridge Crystallographic Data Centre (insert CCDC 2218566-2218570 for L, [**(-)1**]·C_7H_{16}, **[(-)2]$_n$**·nCH_3NO_2, [**(+)1**]·C_7H_{16}, **[(+)2]$_n$**·nCH_3NO_2, respectively). Copies of the data can be obtained, free of charge, on application to the Director, CCDC, 12 Union Road, Cambridge CB2 1EZ, United Kingdom (Fax: 44-1223-336033 or e-mail: deposite@ccdc.cam.ac.uk. X-ray diffraction (XRD) patterns were recorded at room temperature in the 2θ range 5–30° with a step size of 0.026° and a scan time per step of 600 s using a PANalytical X'Pert Pro diffractometer (Cu-L2,L3 radiation, λ = 1.5418 Å, 40 kV, 40 mA, PIXcel 1D detector). Data collector and HighScore Plus software were used, respectively, for recording and analyzing the patterns.

2.4 Spectroscopic Analysis

^{1}H NMR spectra were recorded at room temperature on an AVANCE III 400 BRUKER spectrometer at Centre Régional de Mesures Physiques del'Ouest (CRMPO), Université de Rennes 1. Chemical shifts δ are given in parts per million (ppm) referenced to TMS.

Absorption spectra were recorded on a JASCO V-650 spectrophotometer in diluted solution by using spectrophotometric grade solvents. Electronic circular dichroism (ECD) was measured on a Jasco J-815 Circular Dichroism Spectrometer (IFR140 facility – Biosit-Université de Rennes 1).

3. RESULTS AND DISCUSSION

3.1 Structural Analysis

L ligand. The structure of **L** (Scheme 1) was confirmed by single crystal X-ray diffraction investigation. It crystallizes in monoclinic $P2_1/c$ space group (Table S1). Its Ortep view is depicted in Figure S1 and it ambiguously shows that the substituted pyridine was oxidized in pyridine-*N*-oxide group. The almost planar ligand forms pseudo hydrogen bonds between the NO function and the hydrogen atoms of the pyrazol rings along the *c* axis while the molecules are π-stacked perpendicular to this direction (Figure S2).

[(-)/(+)1]·C_7H_{16}. The reaction between an equimolar of Dy((-)/(+)hfc)$_3$(H_2O) and **L** gave single crystals of **[(-)/(+)1]**·C_7H_{16} (Scheme 1). Only the X-ray structure of the (+) enantiomer is described in the following lines. The phase purity was checked by powder X-ray diffraction (PXRD) at room temperature (Figure S3).

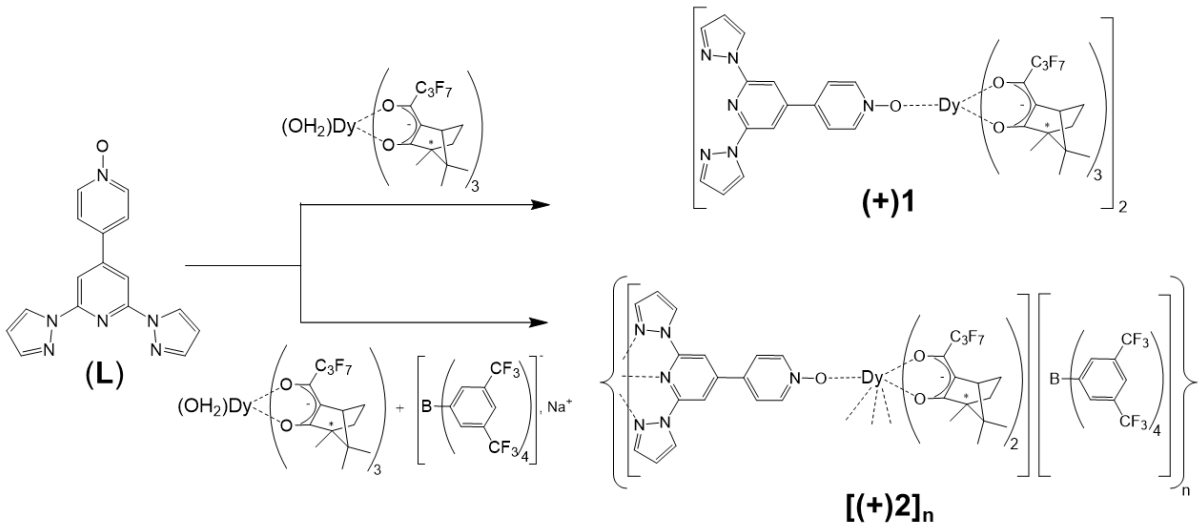

Scheme 1. Molecular structures of the ligand **L** and synthetic routes given the molecular structures for the two pairs of enantiomers **[(-)/(+)1]**·C_7H_{16} and **[(-)/(+)2]$_n$**·nCH_3NO_2. The scheme depicted only the (+) enantiomers.

It crystallizes in the chiral triclinic P1 space group (Table S2) and its asymmetric unit is composed of a dinuclear complex (Figure 1) of formula [Dy((-)/(+)hfc)$_3$(**L**)]$_2$·C_7H_{16} and one *n*-heptane molecule of crystallization. The two crystallographically independent Dy(III) ions are surrounding by three hfc$^-$ anions and two N-O groups coming from **L** ligands. The latter are bridging two Dy(hfc)$_3$ units leading to the formation of a dinuclear complex. The bridging ligands **L** are not planar after complexation with the Dy(hfc)$_3$ with an angle of 41.3° between the dipyrazolylpyridine (dpp) and the 4-pyridine-*N*-oxide moieties. It is worth to notice that the use of an excess of Dy(hfc)$_3$(H_2O) reagent led to the same dinuclear complex. Thus the coordination of **L** through the N-O group is driven by the oxophilic character of the dysprosium and the steric hindrance of the metal precursor. The six hfc$^-$ anion have the same chirality within a dinuclear complex i.e. (-)hfc for **[(-)1]**·C_7H_{16} and (+)hfc for **[(+)1]**·C_7H_{16}. The shortest intra- and intermolecular Dy···Dy distances are 4.178 Å and 11.703 Å, respectively.

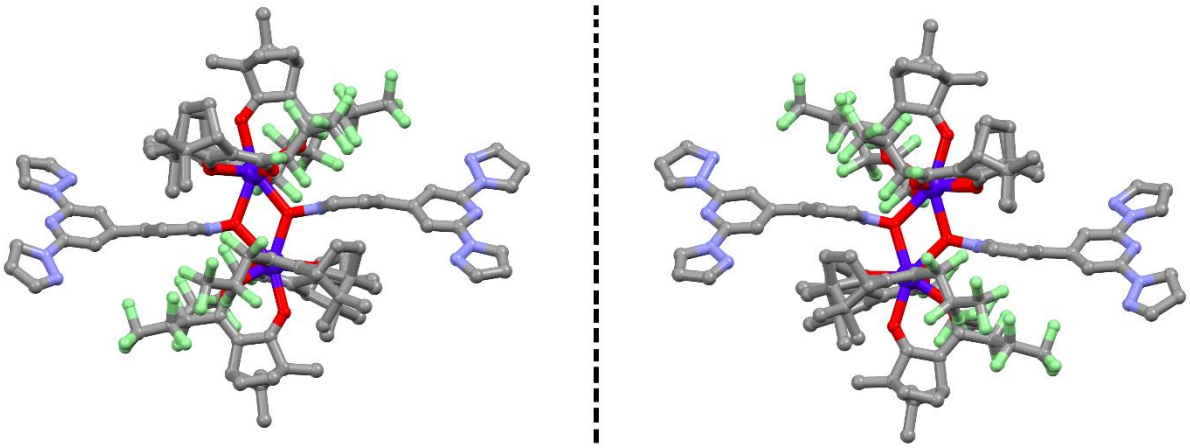

Figure 1. X-ray structures of the two enantiomers **[(-)1]**·C_7H_{16} (left) and **[(+)1]**·C_7H_{16} (right). Hydrogen atoms and *n*-heptane molecule of crystallization are omitted for clarity. Dark blue, Dy; green, F; red, O; blue, N and grey, C.

The crystal packing reveals that the complexes interact through π-π interactions between the dpp moieties (Figure S4) as well as F···F and H···F short contacts.

$[(-)/(+)2]_n$·nCH_3NO_2. The reaction between an equimolar of Dy((-)/(+)hfc)$_3$(H_2O) and **L** in presence of 2 equivalents of NaBarF gave single crystals of **$[(-)/(+)2]_n$**·nCH_3NO_2 (Scheme 1). As for the previous compound, only the X-ray structure of the (+) enantiomer is described in the following lines. It crystallizes in the chiral monoclinic space group P2 (Table S2). The asymmetric unit is composed of two crystallographically independent Dy(III) centers surrounded by five oxygen and three nitrogen atoms coming from two hfc^- anions, one N-O group and the dpp unit of **L** ligand, four half $BArF^-$ anions and two nitromethane solvent molecules of crystallization. Both N-O and dpp moieties come from two different ligands leading to a mono-dimensional coordination polymer (Figure 2). Since only two hfc^- anions are coordinated to the Dy(III), the polymer is cationic. The electro-neutrality is assumed by the presence of one $BArF^-$ anion per Dy(III) center. In other words and to our best knowledge, this is the first observation of the loss of one β-diketonate (hfc^-) anion induced by a non-coordinating anion since usually the anion replaces the lost β-diketonate and remains coordinated to the lanthanide.[15-18] The loss of one hfc^- anion allows the remaining $[Dy(hfc)_2]^+$ cation to be coordinated by the dpp trischelating site. The shortest intra- and intermolecular Dy···Dy distances are 12.681 Å and 13.308 Å, respectively.

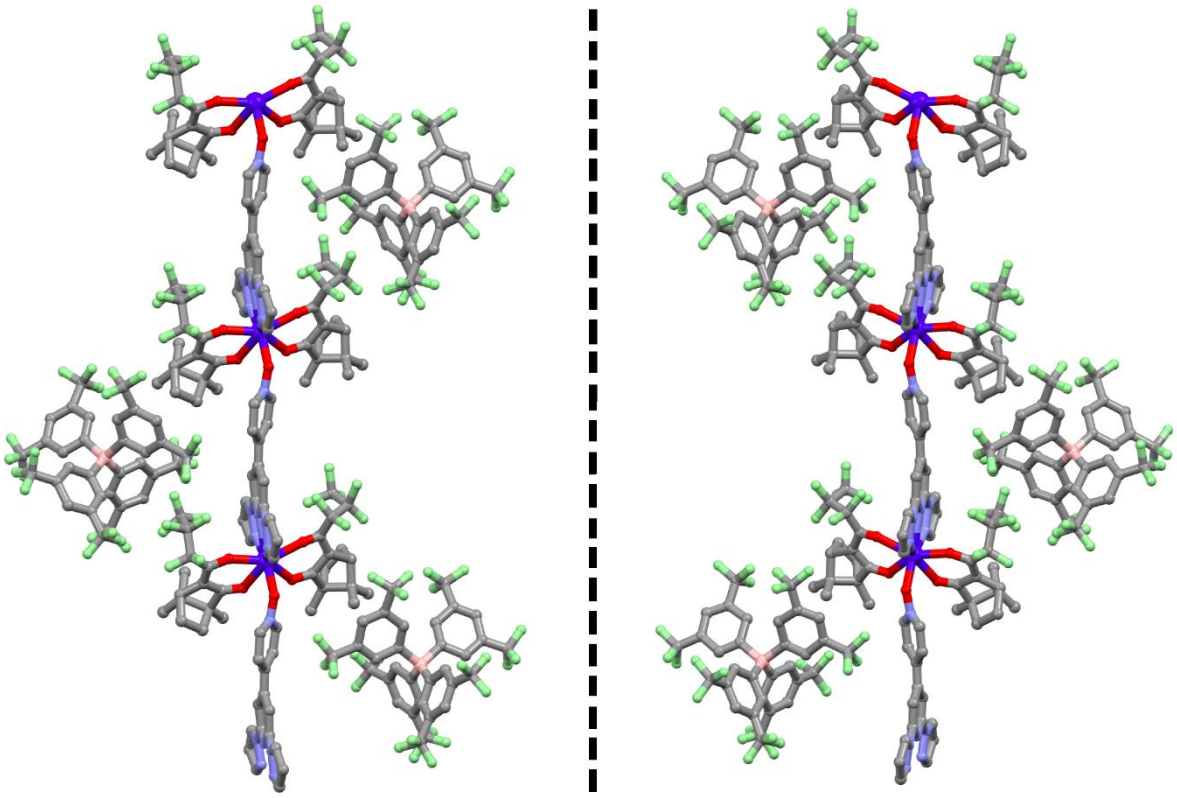

Figure 2. X-ray structures of the two enantiomers **[(-)2]$_n$**·nCH_3NO_2 (left) and **[(+)2]$_n$**·nCH_3NO_2 (right). Hydrogen atoms and nitromethane molecule of crystallization are omitted for clarity. Dark blue, Dy; green, F; red, O; blue, N; salmon, B and grey, C.

The crystal packing reveals that the 1D cationic coordination polymers are well shielded by the four crystallographically independent bulky $BarF^-$ anions (Figure S5). All the hfc^- anions of the crystal have the same chirality depending of the studied enantiomers.

3.2 Optical Analysis: UV-visible Absorption and CD measurements

The UV-visible absorption and Natural Circular Dichroism (NCD) spectra for the complexes **[(-)/(+)1]** and **[(-)/(+)2]$_n$** have been measured in CH_2Cl_2 solution (Figure 3). The experimental absorption curves for the two enantiomers of each complexes are composed of broad bands localized at 280-350 nm and attributed to the (+)/(-)hfc^- anions.[30] For **[(-)/(+)1]** the absorption band at high wavelength (250 nm) can mainly attributed to the π–π* transitions of the **L** ligand while **[(-)/(+)2]$_n$** displayed additional absorption contribution which could be attributed to contribution of the π–π* transitions of the $BarF^-$ anions. The largest absolute values of the dissymmetry factor $|g_{abs}|$ display magnitude order of 5×10^{-4} at 295 nm for **[(-)/(+)1]** and 1×10^{-3} at 300 nm for **[(-)/(+)2]** (Equation 1):

$g_{abs} = \Delta\varepsilon/\varepsilon = (\varepsilon_L - \varepsilon_R)/(1/2(\varepsilon_L + \varepsilon_R))$ eq. 1

where $\Delta\varepsilon = \varepsilon_L - \varepsilon_R$ is the difference between the left (ε_L) and right (ε_R) molar absorption coefficients at the absorption wavelength.

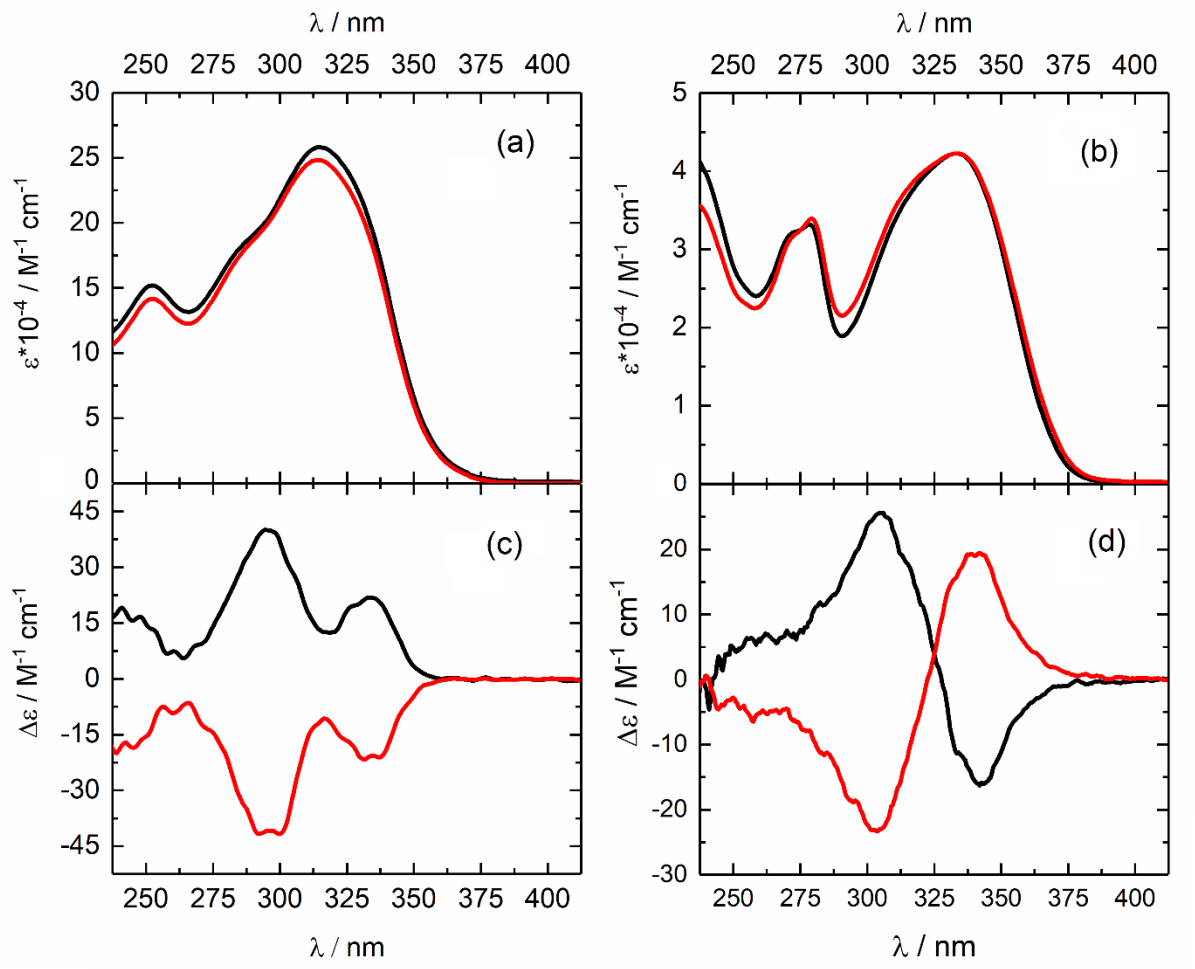

Figure 3. Absorption spectra of **[(-)/(+)1]** (a) and **[(-)/(+)2]$_n$** (b) in CH_2Cl_2 (C = 1×10^{-4} M) and the respective natural circular dichroism spectra for **[(-)/(+)1]** (c) and **[(-)/(+)2]$_n$** (d) in CH_2Cl_2 (C = 1×10^{-4} M). (-) and (+) enantiomers are depicted respectively in red and black.

The measurements of NCD show mirror images of the spectra which confirm the enantiomeric nature of the complexes in CH_2Cl_2 solution at room temperature. A correspondence between the NCD and absorption bands can be observed since only the electronic excitations attributed to hfc^- anions gave CD activity. NCD spectra mainly exhibit two negative (for **[(-)1]**) and positive (for **[(+)1]**) contributions at 295 nm and 330 nm (Figure 3c). In case of **[(-)/(+)2]$_n$**, CD contributions are observed at similar wavelength than for **[(-)/(+)1]** but a classic exciton CD couplet with a negative and positive sign is identified (Figure 3d). The exciton CD couplet is due to the helical dispositions of the ligands around the

lanthanide center as observed for the tetrakis and tris bidentate β-diketonate complexes i.e. square antiprism (SAPR). It is well-known than for such complexes, the presence or not of the exciton CD couplet is also dependent of the solvent[30] and the concentration[31]. In the present case, solvent and concentration are identical for both pairs of enantiomers, thus the absence of the exciton CD couplet for **[(-)/(+)1]** suggests the absence of the Λ/Δ SAPR-8 configuration while it remains for **[(-)/(+)2]$_n$** in CH_2Cl_2 solution (C = 10^{-4} M).

3.3 Magnetic properties

3.3.1 Static dc magnetic measurements

The magnetic properties for two enantiomers are expected to be rigorously identical, consequently only the (+) enantiomer of the dinuclear and 1D compounds have been studied. The room temperature values of the $\chi_M T$ product (where χ_M is the magnetic susceptibility) are 27.92 cm^3 K mol^{-1} for **[(+)1]** (Figure S8) and 13.97 cm^3 K mol^{-1} for **[(+)2]$_n$** (Figure S9) which are in agreement with the expected values of 28.34 cm^3 K mol^{-1} for two and one isolated Dy(III) ion ($^6H_{15/2}$ ground state),[32] respectively. The thermal dependences of the product $\chi_M T$ for **[(+)1]** and **[(+)2]$_n$** present a continuous decrease lowering the temperature and reaching values of 15.86 cm^3 K mol^{-1} and 11.46 cm^3 K mol^{-1} respectively. Such decrease is mainly attributed to the depopulation of the M_J doublet when lowering the temperature for **[(+)2]$_n$** since the presence of antiferromagnetic interaction can be reasonably excluded taking into account of the long distances between the Dy(III) ions in the crystal structure while for **[(+)1]** additional intramolecular antiferromagnetic dipolar and exchange interactions between the two Dy(III) are expected as already observed in similar dinuclear complexes.[33-35] The field dependences of the magnetization are depicted in inset of the Figures S8 and S9. At 50 kOe, M(H) take the values of 10.29 Nβ for **[(+)1]** and 5.67 Nβ for **[(+)2]$_n$** which are far from the expected theoretical saturation values sign of significant magnetic anisotropy in both molecular systems. Magnetizations loops have been measures on **[(+)1]** in the 0.5-4 K temperature range.

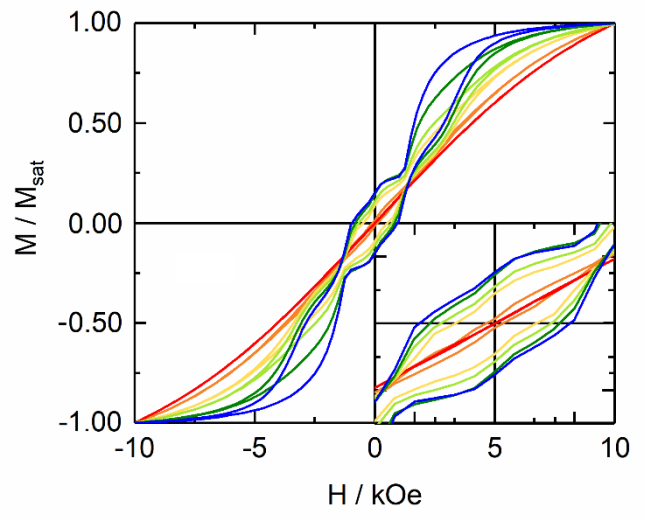

Figure 4. Normalized magnetic hysteresis loops at 0.5 K (blue), 1 K (dark green), 1.5 K (green), 2 K (yellow), 3 K (orange) and 4 K (red) and a sweep rate of 16 Oe s^{-1} for **[(+)1]**. Inset, zoom view of the origin zone.

At zero field the hysteresis is open with a coercitive field of 2000 Oe which is a higher value than the ones extracted for similar dinuclear complexes involving other β-diketonate.[33-35] As the field is applied, the hysteresis loop opens slightly more (2200 Oe at 1000 Oe). It then narrows significantly (250 Oe at 1500 Oe) because of the level crossing between the first excited and ground states. Last, once the crossing field is overwhelmed the hysteresis re-opens (1350 Oe at 2500 Oe) to finally close around 7500 Oe.

3.3.2 Dynamic ac magnetic measurements

Dynamic studies of the magnetization were investigated on both **[(+)1]** and **$[(+)2]_n$** samples. In zero applied magnetic field, only **[(+)1]** shows clear out-of-phase (χ_M'') maxima (Figures 5 and S10). In-phase and out-phase components of the magnetic susceptibility are simultaneously fitted using an extended Debye model (Table S3). The obtained α values are in the range 0.06-0.24 from low to high temperature sign of a single magnetic relaxation process except for cryogenic temperature. The normalized Argand plot (Figure S11) confirmed that the slow magnetic relaxation fraction represents the entire sample. The magnetic relaxation time τ was extracted and its thermal evolution plots in Figure 5b. The log(τ) vs T plot was fitted using the equation 1:

$$\tau^{-1}(T,H) = AH^4T + \frac{B_1}{1+B_2H^2} + \underbrace{\tau_0^{-1} e^{\left(\frac{U_{eff}}{k_B T}\right)}}_{k(T)} + CT^n \qquad \text{Eq 1.}$$

From left to right, the terms are the expressions of Direct, QTM and thermally activated (Orbach + Raman) contributions. The best fit was obtained using a combination of QTM and Raman processes with the following parameters τ_{TI} = 42.7(8) s^{-1}, C = 1.34(18) × 10^{-4} s K^{-n} with n = 5.87(6). The n value is in agreement with the expected values for Kramers ions.[36,37] To optimize the magnetic performances of the SMM, it well known that the QTM could be cancelled by applying an external dc field. From the hysteresis loops of **[(+)1]** (Figure 4), one could conclude that 1000 Oe is a suitable value. In such applied magnetic field, a frequency dependence of the magnetic susceptibility is kept (Figures 5c and S12) and the thermal variation of the extracted τ using the extended Debye model (Table S4) can be fitted using the same equation 1 (Figure 5d). The best fit was found using a Raman process only with parameters (C = 2.61(19) × 10^{-4} s K^{-n} with n = 5.61(4)) very close to those found under 0 Oe applied field. In other word, the 1000 Oe dc field efficiently suppressed the QTM. The normalized Argand attested that the whole sample is slowly relaxing under an applied dc field of 1000 Oe.

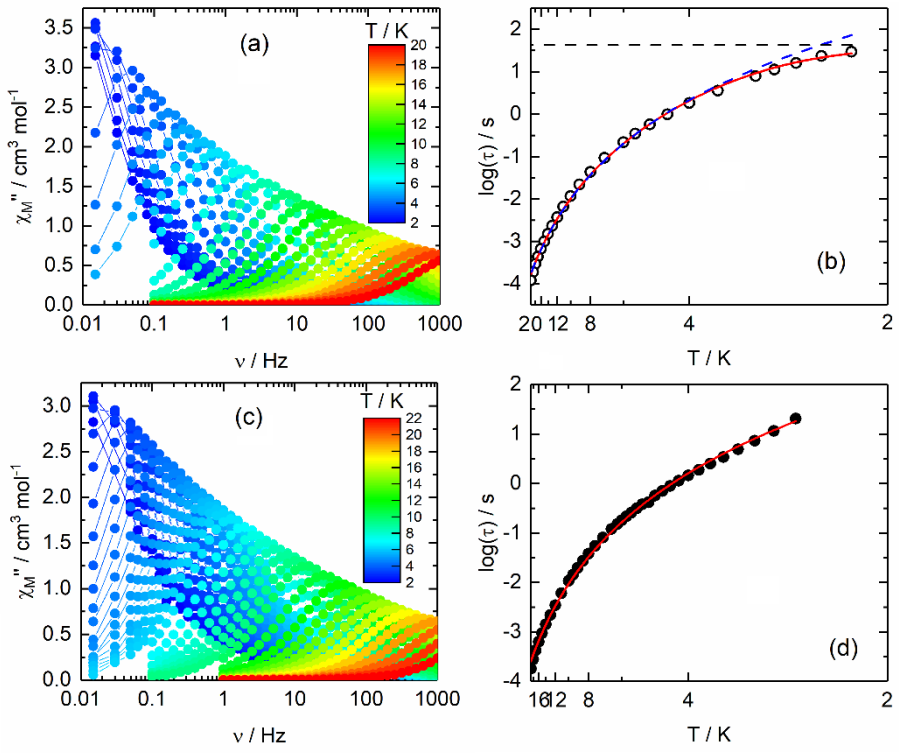

Figure 5. Frequency dependence of χ_M'' at 0 Oe in the temperature range 2-20 K (a) and at 1000 Oe in the temperature range 2-22 K (c) for **[(+)1]**. Temperature variations of the relaxation times in the range 2.2-22 K under 0 Oe (open circles) and in the range of 2.6-19 K

under 1000 Oe (full black circles) for **[(+)1]**. The red lines depict the best fits by considering QTM (dashed black line) + Raman (dashed blue line) relaxation processes at 0 Oe and Raman process only at 1000 Oe. Parameters given in the text.

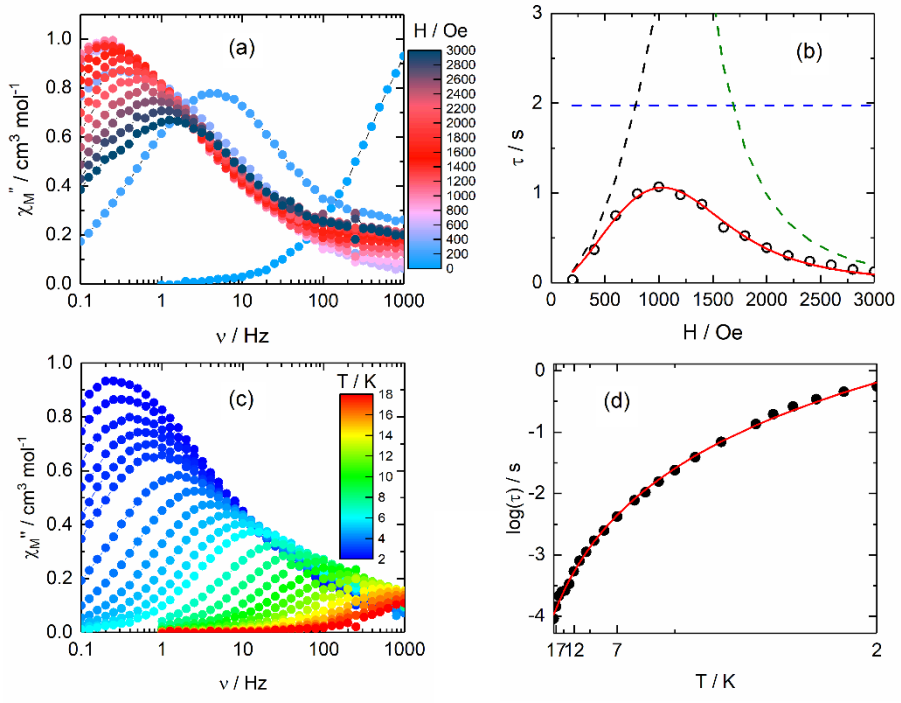

Figure 6. Frequency dependence of χ_M'' between 0 and 3000 Oe at 2 K for **[(+)2]$_n$** (a). Field dependence of the relaxation times for **[(+)2]$_n$** (open circles) (b) between 200 and 3000 Oe at 2 K. Red line is the best fitted curve. Each relaxation process is represented as follow: QTM (black dashed line), Direct (green dashed line) and thermally activated k(T) contribution (blue dashed line). Parameters given in the text. Frequency dependence of χ_M'' at 800 Oe in the temperature range 2-18 K for **[(+)2]$_n$** (c). Temperature variations of the relaxation times in the range 2-18 K under 800 Oe (full black circles) (d). The red lines depict the best fits with parameters given in the text.

In case of **[(+)2]$_n$**, a field dependence of the magnetic susceptibility was investigated (Figures 6a and S14). As soon as a dc field is applied, the χ_M'' shifts to lower frequency. Whatever the value of the applied dc field, a single χ_M'' contribution is observed indicating the absence of significant dipolar interaction in agreement with crystal structure.[38] The relaxation times were extracted at any dc field value using the extended Debye model (Table S5) and plot in Figure 6b. The magnetization relaxation rate initially decrease with increasing the field until reaching a minimum value and then increases at higher dc field values. Such

behavior is coherent with relaxation via QTM at low static magnetic field followed by the activation of a direct mechanism for stronger fields. The τ *vs* H plot was fitted with the equation 1. The best fit was obtained with the following parameters: $B_1 = 6.0(9) \times 10^4$ s^{-1}, $B_2 = 1.9(3) \times 10^{-2}$ Oe^{-2}, $A = 6.4(8) \times 10^{-14}$ s^{-1} K^{-1} Oe^{-4} and $k(T) = 0.51(2)$ s^{-1} (Figure 6b). Thus the value of 800 Oe was selected to study the temperature dependent behavior of the magnetic susceptibility for **[(+)2]$_n$** (Figures 6c and S15). Under such dc field, the magnetic susceptibility displays a clear frequency dependence for which both QTM and direct processes could be discarded from the analysis of the field dependence of τ. The normalized Argand indicates that the out-of-phase component of the magnetic susceptibility involves 70 % of the sample at 2K (Figure S16). The magnetic relaxation times at 800 Oe were extracted using the extended Debye model (Table S6). The log(τ) vs T plot was fitted using the equation 1 (Figure 6d). The best fit was found using a Raman process only with the parameters $C = 9.94(1) \times 10^{-2}$ s K^{-n} with n = 3.97(3).

4. CONCLUSION

In conclusion, two unprecedented chiral dinuclear complex and chiral mono-dimensional cationic coordination polymer of respective formula $[Dy((-)/(+)hfc)_3(\mathbf{L})]_2 \cdot C_7H_{16}$ (**[(-)/(+)1]·C_7H_{16}**) and $\{[Dy((-)/(+)hfc)_2(\mathbf{L})][BarF]\}_n \cdot nCH_3NO_2$ (**[(-)/(+)2]$_n$·nCH_3NO_2**) were obtained by reaction of an equimolar quantities of enantiopure $[Dy((-)/(+)hfc)_3(H_2O)]$ and the 4′-(4′′′-pyridyl-*N*-oxide)-1,2′:6′1′′-bis-(pyrazolyl)pyridine] (**L**) ligand respectively in absence and presence of sodium tetrakis[3,5-bis(trifluoromethyl)phenyl]borate salt (NaBArF). Natural circular dichroism (NCD) highlighted an exciton CD couplet for **[(-)/(+)2]$_n$** due to the helical dispositions of the ligands while such feature was not observed for **(-)/(+)1**. However the latter displayed remarkable magnetic behavior with a Single-Molecule Magnet (SMM) behavior and a magnetic bistability up to 4 K. The remaining Quantum Tunneling of the Magnetization (QTM) not cancelled by the magnetic interaction can be suppressed by an 1000 Oe external dc field leading to a magnetic relaxation through a Raman process only. **[(-)/(+)2]$_n$** displayed a slow magnetic relaxation under an applied magnetic field of 800 Oe and a magnetic relaxation through Raman process only too. Our synthetic strategy showed that chiral SMM could be obtained by partial dissociation of the chiral $[Dy((-)/(+)hfc)_3(H_2O)]$ in presence of non-coordinating bulky anions.

ACKNOWLEDGEMENTS

This work was supported by CNRS, Université de Rennes and the European Research Council through the ERC-CoG 725184 MULTIPROSMM (project no. 725184). Part of this work has been performed using the Spectroscopies-DCTP core facility (UMS Biosit, Université de Rennes 1- Campus de Villejean - 35043 RENNES Cedex, FRANCE).

REFERENCES

1. Woodruff DN, Winpenny REP, Layfield RA. Lanthanide Single-Molecule Magnets. *Chem. Rev.* 2013;113(7):5110–5148.
2. de Bettencourt-Dias A. Luminescence of lanthanide ions in coordination compounds and nanomaterials, John Wiley & Sons, Ltd, 2014.
3. Guo FS, Day BM, Chen YC, Tong ML, Mansikkamäki A, Layfield RA. Magnetic hysteresis up to 80 kelvin in a dysprosium metallocene single-molecule magnet. *Science* 2018;362(6421):1400–1403.
4. Mannini M, Pineider F, Sainctavit P, et al. Magnetic memory of a single-molecule quantum magnet wired to a gold surface. *Nat. Mater.* 2009;8(3):194−197.
5. Long J, Ivanov MS, Khomchenko, VA, et al. Room temperature magnetoelectric coupling in a molecular ferroelectric ytterbium(III) complex. *Science* 2020;367(6478):671-676.
6. Wang K, Zeng S, Wang H, Dou J, Jiang J. Magneto-chiral dichroism in chiral mixed (phtalocyaninato)porphyrinato) rare earth triple-decker SMMs. *Inorg. Chem. Front.* 2014;1:167-171.
7. Atzori, M, Dhbaibi K, Douib H, et al. Helicene-Based Ligands Enable Strong Magneto-Chiral Dichroism in a Chiral Ytterbium Complex. *J. Am. Chem. Soc.* 2021;143(7):2671-2675.
8. Liu CM, Zhang DQ, Zhu DB. Field-Induced Single-Ion Magnets Based on Enantiopure Chiral β-Diketonate Ligands. *Inorg. Chem.* 2013;52(15):8933-8940.
9. Li DP, Wang TW, Li CH, Liu DS, Li YZ, You XZ. Single-ion magnets based on mononuclear lanthanide complexes with chiral Schiff base ligands $[Ln(FTA)_3L]$ (Ln = Sm, Eu, Gd, Tb and Dy). *Chem. Commun.* 2010;46:2929-2931.
10. Ou-Yang, JK, Saleh N, Fernández García, G, et al. Improved slow magnetic relaxation in optically pure helicene-based Dy^{III} single molecule magnets. Chem. Commun. 2016;52:14474-14477.

11. Feng M, Lyu BH, Wang MH, et al. Chiral Erbium(III) Complexes : Single-Molecule Magnet Behavior, Chirality, and Nuclearity Control. *Inorg. Chem.* 2019;58(16):10694-10703.
12. Muller G. Luminescent chiral lanthanide(III) complexes as potential molecular probes. *Dalton Trans.* 2009:9692-9707.
13. Gendron F, Di Pietro S, Abad Galan L, et al. Luminescence, chiroptical, magnetic and ab initio crystal-field characterizations of an enantiopure helicoidal Yb(III) complex. *Inorg. Chem. Front.* 2021;8:914-926.
14. Pointillart F, Maury O, Le Gal Y, Golhen S, Cador O, Ouahab L. 4-(2-Tetrathiafulvalene-ethenyl)pyridine (TTF-CH=CH-Py) Radical Cation Salts Containing Poly(β-diketonate) Rare Earth Complexes: Synthesis, Crystal Structure, Photoluminescent and Magnetic Properties. *Inorg. Chem.* 2009;48:7421-7429.
15. Alvarez Vicente J, Mlonka A, Nimal Gunaratne HQ, Swadzba-Kwasny M, Nockemann P. Phosphine oxide functionalized imidazolium ionic liquids as tunable ligands for lanthanide complexation. *Chem. Commun.* 2012;48:6115-6117.
16. Onghena B, Jacobs J, Van Meervelt L, Binnemans K. Homogeneous liquid-liquid extraction of neodymium(III) by choline hexafluoroacetylacetonate in the ionic liquid choline bis(trifluoromethylsulfonyl)imide. *Dalton Trans*. 2014;43:11566-11578.
17. Pointillart F, Cauchy T, Maury O, et al. Tetrathiafulvalene-amido-2-pyridine-N-oxide as Efficient Charge-Transfer Antenna Ligand for the Sensitization of Yb^{III} Luminescence in a Series of Lanthanide Paramagnetic Coordination Complexes. *Chem. Eur. J.* 2010;16:11926-11941.
18. Pointillart F, Le Guennic B, Golhen S, Cador O, Ouahab L. Slow magnetic relaxation in radical cation tetrathiafulvalene-based lanthanide(III) dinuclear complexes. *Chem. Commun.* 2013;49:11632-11634.
19. Feng M, Pointillart F, Lefeuvre B, et al. Multiple Single-Molecule Magnet Behaviors in Dysprosium Dinuclear Complexes Involving a Multiple Functionalized Tetrathiafulvalene-Based Ligand. *Inorg. Chem.* 2015;54:4021-4028.
20. Halcrow MA. Iron(II) complexes of 2,6-di(pyrazol-1-yl)pyridines-A versatile system for spin-crossover research. *Coord. Chem. Rev.* 2009;253(21-22):2493-2514.
21. Douib H, Cornet L, Flores Gonzalez J, et al. Spin-Crossover and Field-Induced Single-Molecule Magnet Behaviour in Metal(II)-Dipyrazolylpyridine Complexes. *Eur. J. Inorg. Chem.* 2018:4452-4457.

22. Pointillart F, Le Gal Y, Golhen S, Cador O, Ouahab L. 4f Gadolinium(III) Complex Involving Tetrathiafulvalene-amido-2-pyrimidine-1-oxide as a Ligand. *Inorg. Chem.* 2009;48:4631-4633.
23. Pointillart F, Le Guennic B, Golhen S, Cador O, Maury O, Ouahab L. High Nuclearity Complexes of Lanthanide Involving Tetrathiafulvalene Ligands: Structural, Magnetic, and Photophysical Properties. *Inorg. Chem.* 2013;52:1610-1620.
24. Pointillart F, Guizouarn T, Lefeuvre B, Golhen, S, Cador O, Ouahab L. Rational Design of a Lanthanide-Based Complex Featuring Different Single-Molecule Magnets. *Chem. Eur. J.* 2015;21:16929-16934.
25. Ghosh I, Zeng H, Kishi Y. Application of Chiral Lanthanide Shift reagents for Assignment of Absolute Configuration of Alcohols. *Org. Lett.* 2004;6(25):4715-4718.
26. Rajadurai C, Schramm F, Drink S, et al. Spin transition in a Chainlike Supramolecular Iron(II) Complex. *Inorg. Chem.* 2006;45(25):10019-10021.
27. Sheldrick GM. SHELXT – Integrated space-group and crystal-structure determination *Acta Crystallogr., Sect. A: Found. Adv.* 2015;71:3-8.
28. Sheldrick GM. Crystal structure refinement with SHELXL. *Acta Crystallogr. Sect. C* 2015;71:3-8.
29. Spek AL. Single-crystal structure validation with the program PLATON. *J. Appl. Crystallogr.* 2003;36;7-13.
30. Shirotani D, Susuki T, Yamanari K, Kaizaki S. Crystal structure and chiroptical spectra of sodium tetrakis(+)-hfbc Pr(III) complex. *J. Alloys Compd.* 2008;451:325-328.
31. Lunkley JL, Shirotani D, Yamanari K, Kaizaki S, Muller G. Extraordinary Circularly Polarized Luminescence Activity Exhibited by Cesium Tetrakis(3-heptafluoro-butylryl-(+)-camphorato) Eu(III) Complexes in EtOH and $CHCl_3$ Solutions. *J Am Chem Soc.* 2008;130(42):13814–13815.
32. Kahn O. *Molecular Magnetism*, VCH, Weinhem, 1993.
33. Pointillart F, Le Guennic B, Maury O, Golhen S, Cador O, Ouahab L. Lanthanide Dinuclear Complexes Involving Tetrathiafulvalene-3-pyridine-N-oxide Ligand: Semiconductor Radical Salt, Magnetic, and Photophysical Studies. *Inorg. Chem.* 2013;52(3):1398–1408
34. Guo YN, Xu GF, Wernsdorfer W, et al. Strong Axiality and Ising Exchange Interaction Suppress Zero-Field Tunneling of Magnetization of an Asymmetric Dy_2 Single-Molecule Magnet. *J. Am. Chem. Soc.* 2011;133(31):11948–11951

35. Chow CY, Bolvin H, Campbell VE, et al. Assessing the exchange coupling in binuclear lanthanide(III) complexes and the slow relaxation of the magnetization in the antiferromagnetically coupled Dy2 derivative. *Chem. Sci.* 2015;6:4148-4159.
36. Dekker C, Arts AFM, de Wijn HW, van Duyneveldt AJ, Mydosh JA. Activated dynamics in a two-dimensional Ising spin glass: $Rb_2Cu_{1-x}Co_xF_4$. *Phys. Rev. B: Condens. Matter Mater. Phys.* 1989;40:11243–11251.
37. Tang J, Zhang P. *Lanthanide Single Molecule Magnets*, Springer-Verlag: Berlin, 2015.
38. Pointillart F, Bernot K, Golhen S. Magnetic Memory in an Isotopically Enriched and Magnetically Isolated Mononuclear Dysprosium Complex. *Angew. Chem. Int. Ed.* 2015;54(5):1504-1507.